Color Centers



www.advmat.de

Improving Defect-Based Quantum Emitters in Silicon **Carbide via Inorganic Passivation**

Mark J. Polking, Alan M. Dibos, Nathalie P. de Leon, and Hongkun Park*

Defect-based color centers in wide-bandgap crystalline solids are actively being explored for quantum information science, sensing, and imaging. Unfortunately, the luminescent properties of these emitters are frequently degraded by blinking and photobleaching that arise from poorly passivated host crystal surfaces. Here, a new method for stabilizing the photoluminescence and charge state of color centers based on epitaxial growth of an inorganic passivation layer is presented. Specifically, carbon antisite-vacancy pairs (CAV centers) in 4H-SiC, which serve as single-photon emitters at visible wavelengths, are used as a model system to demonstrate the power of this inorganic passivation scheme. Analysis of CAV centers with scanning confocal microscopy indicates a dramatic improvement in photostability and an enhancement in emission after growth of an epitaxial AIN passivation layer. Permanent, spatially selective control of the defect charge state can also be achieved by exploiting the mismatch in spontaneous polarization at the AIN/SiC interface. These results demonstrate that epitaxial inorganic passivation of defect-based quantum emitters provides a new method for enhancing photostability, emission, and charge state stability of these color centers.

Defect-based color centers in a solid-state crystal represent a promising class of quantum emitters. When their energy levels lie within the bandgap of a host material, localized defects can provide room-temperature single-photon emission with exceptional quantum yield, [1,2] enabling new applications in quantum optics,[3-9] imaging,[10] and sensing.[11] Charge traps arising from unpassivated surface states, surface adsorbates, and damage induced by nanofabrication can cause the deterioration of the optical properties of color centers, leading to blinking, photobleaching, and the destabilization of the emissive charge state.[12,13] Although molecular termination schemes have been explored in some host materials to protect and passivate the surface, [13] these schemes are neither chemically nor thermally stable,[14,15] limiting their potential for applications requiring long-term stability.

Dr. M. J. Polking, [+] Dr. A. M. Dibos, [++] Dr. N. P. de Leon, [++] Prof. H. Park Department of Chemistry and Chemical Biology Harvard University

Cambridge, MA 02138, USA

E-mail: hongkun_park@harvard.edu

Dr. N. P. de Leon, Prof. H. Park

Department of Physics

Harvard University

Cambridge, MA 02138, USA

[+] Present address: Physical Sciences Inc., Andover, MA 01810, USA [++]Present address: Department of Electrical Engineering, Princeton University, Princeton, NJ 08544, USA

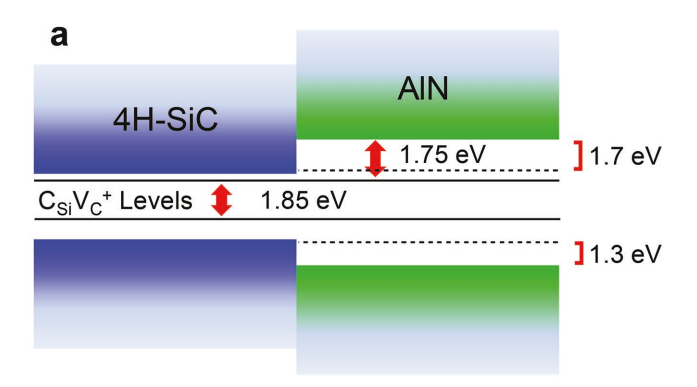
DOI: 10.1002/adma.201704543

Here, we demonstrate a new strategy to preserve and improve the optical properties of defect-based color centers via epitaxial growth of wide-bandgap inorganic materials, in analogy to well-established passivation schemes in III-V quantumwell structures and core-shell semiconductor quantum dots.[16] As a proof of principle, we apply this new scheme to the recently discovered carbon antisitevacancy (CAV) pair in 4H-SiC,[2,17] which has been shown to act as a room-temperature single-photon source at visible wavelengths. [2] We grow epitaxial passivation layers of wurtzite aluminum nitride (AlN) on 4H-SiC by radio frequency (RF) sputtering and demonstrate their crystal quality and epitaxy by high-resolution transmission electron microscopy (HRTEM) and Fourier transform infrared spectroscopy (FTIR). We further show via confocal photoluminescence (PL) microscopy that, after the epitaxial protection,

the color centers exhibit enhanced emission and substantial improvement in photostability. Finally, we demonstrate that, in these polar AlN/4H-SiC heterostructures, the spontaneous polarization of the host material enables charge-state stabilization and spatial control of defect emission. This work represents the first application of epitaxial inorganic passivation schemes to defect-based quantum emitters and provides a promising route toward robust single-photon sources with improved photostability and permanent, spatially selective charge-state control.

The CAV pair in 4H-SiC consists of a carbon atom on a silicon lattice site next to a vacancy on a carbon lattice site.[2,17] CAV pairs can exist in multiple spatial configurations with zero phonon lines in the 670-690 nm range and, at room temperature, exhibit broadband PL over a wavelength range of 650-800 nm. Previous calculations using density functional theory indicate that this PL arises from positively charged CAV pairs with a ground (excited) state 1.9 (0.05) eV beneath the conduction band minimum, as illustrated in Figure 1a.[2] The CAV pairs used in our experiment were created by electron irradiation (2 MeV energy) of high-purity semi-insulating 4H-SiC substrates followed by high-temperature annealing, as reported previously^[2] (details of our sample preparation procedures can be found in the Experimental Section).

AlN with the hexagonal wurtzite structure provides an ideal material for structurally and electronically passivating the surface of hexagonal 4H-SiC and stabilizing its color centers. The bandgap of AlN (6.2 eV) is much larger than that of 4H-SiC



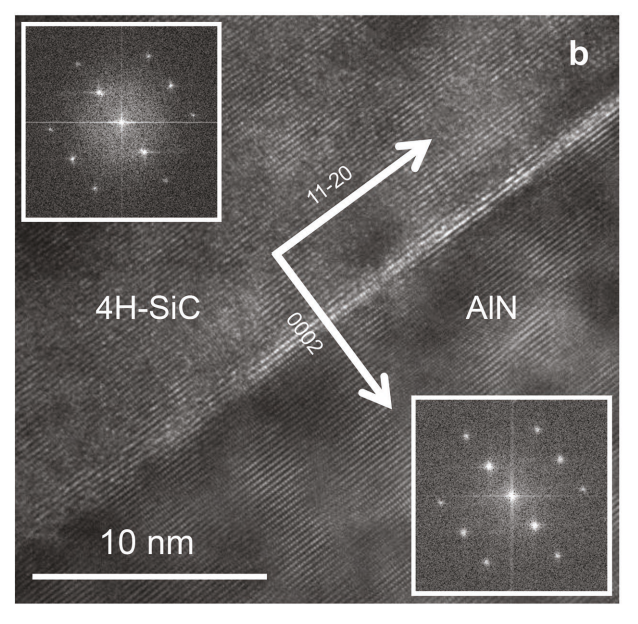


Figure 1. Band alignments and high-resolution transmission electron microscope (HRTEM) images of AlN/4H-SiC heterostructures. a) Band alignments for AlN/4H-SiC heterostructures. The bandgaps of 4H-SiC and AlN are 3.2 and 6.2 eV, respectively. The positions of the localized energy levels of positively charged carbon antisite-vacancy pairs in SiC are also illustrated. b) Typical HRTEM image of an epitaxial AlN film grown on a [0001]-oriented 4H-SiC substrate.

(3.2 eV), and the lattice spacing of AlN (3.07 Å in the basal plane) is closely matched with that of 4H-SiC (3.11 Å), enabling effective removal of surface states and high-quality epitaxial growth.[18,19] Previous measurements of the band alignments (Figure 1a) indicate a clear type-I heterostructure with substantial potential barriers, thereby preventing transfer of photogenerated charges to the outer AlN surface. [18] High-quality epilayers of AlN have previously been grown on 4H-SiC substrates by molecular beam epitaxy (MBE).[19,20] Growth of AlN films has also been demonstrated using reactive DC sputtering of an aluminum target.^[21] In our experiment, 5 nm thick films of AlN were grown on both [0001] and [000-1] oriented 4H-SiC substrates via RF sputtering of a stoichiometric AlN target at 500 °C under a 5% N₂/95% Ar atmosphere. This RF sputtering technique features a slower growth rate compared to DC reactive sputtering, thus allowing for controlled growth of thin layers. Analyses of FTIR reflectance data (Figure S1, Supporting Information) and HRTEM images indicate high-quality epitaxy

of wurtzite AlN on SiC with the <0001> directions aligned in parallel (Figure 1b; Figures S2 and S3, Supporting Information).^[22] In addition, HRTEM images of the AlN-SiC interface (Figures S4 and S5, Supporting Information) indicate coherence of lattice planes across the interface and sub-nm interfacial roughness.

The CAV centers were characterized using scanning confocal PL microscopy before and after AlN epilayer growth under 3 mW laser excitation at 532 nm (Figure 2). The CAV centers were found only near the SiC surface (Figure S6, Supporting Information), consistent with the previous findings of Castelletto et al.^[2] The origins of this behavior are presently unclear. Scanning PL measurements reveal that, whereas the count rates of the CAV centers on the nonequivalent Si face (0001) and the C face (000-1) of 4H-SiC are similar before passivation, their behaviors change dramatically upon AlN epilayer growth.

Specifically, confocal microscopy scans reveal that the brightness of the CAV centers on the AlN-passivated C face increases dramatically compared to those of bare C-face SiC (Figure 2c,d). In contrast, the brightness of the CAV centers on the AlN-passivated Si face (Figure 2b) is reduced from the intensity of those on the bare surface (and also to the AlN-passivated C face). Spectra of C-face CAV centers after AlN passivation show emission ranging from 620 to 800 nm with a peak at around 680 nm (Figure S7, Supporting Information), consistent with roomtemperature PL data reported previously.[2] Moreover, photon correlation measurements ($g^2(\tau)$) of these centers (Figure 2d, inset) are consistent with single-photon emitters, although obtaining a $g^2(0)$ signal less than 0.5 proved difficult due to a strong diffuse background likely stemming from spatially unresolvable CAV centers. The reduction in PL on the Si face after AlN passivation rules out the possibility that the increase in emission originates from emitters in the AlN layer. This is also consistent with the fact that oxygen-related defects in AlN emit photons in the range of 350-550 nm, well outside the range of the optical filters used for our measurements.[23]

Analysis of CAVs on the AlN-passivated C face reveals a substantial improvement in photostability compared to their unpassivated counterparts. We focus our analysis on the C-face centers, which maintain strong PL emission after the AlN epilayer growth. Quantitative analysis of 60 s time traces collected for individual CAVs demonstrates a decrease in blinking and photobleaching after AlN deposition. Example time traces and composite histograms of absolute count values before and after passivation are shown in Figure 3 and Figure S8 (Supporting Information), respectively. Figure 3a,b, which shows composite count histograms representing normalized count values (background as 0 and "on" state count levels as 1) obtained from 50 separate CAVs (with 60 s time traces with 5 ms resolution), clearly demonstrates the large improvement in photostability after passivation. Prior to passivation, the mean normalized count value (N = 50 CAVs) is 0.03 ± 0.48 (the error denotes one standard deviation), indicating rapid photobleaching of CAVs. After AlN epilayer deposition, the mean normalized count level (N=50) improves to 0.80 ± 0.57 under the same excitation conditions. Further improvement in the photostability is observed when lower energy excitation at 660 nm (3 mW laser power) is used. Analysis of time traces (Figure 3c,d) yields an improved value of the normalized

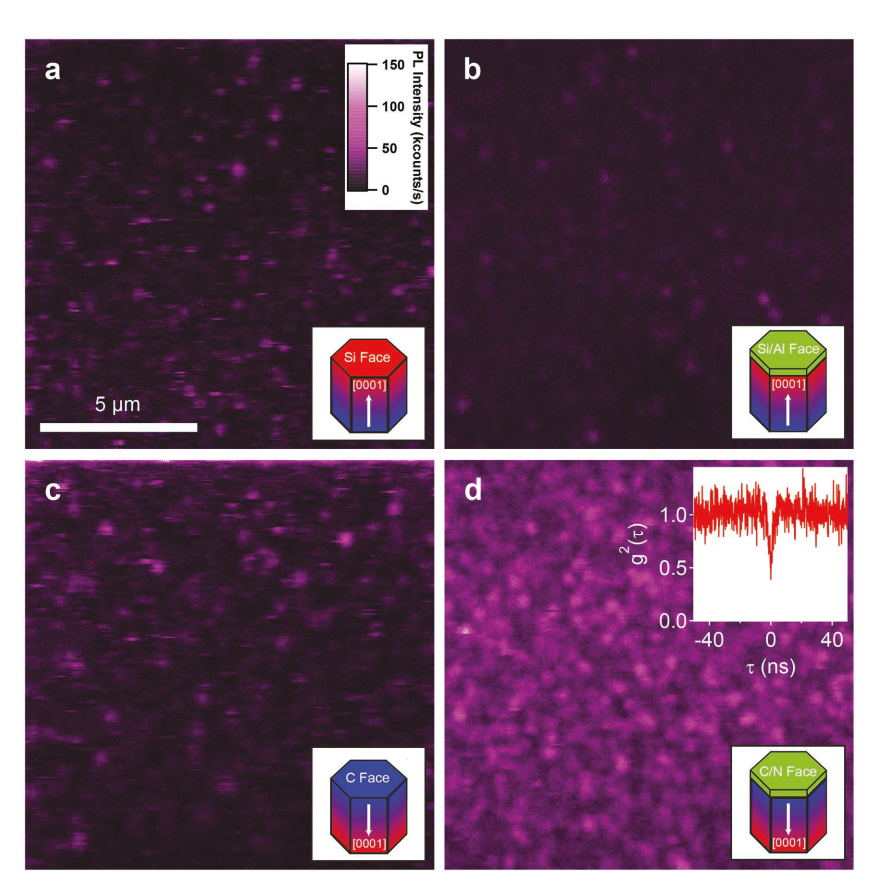


Figure 2. Scanning confocal photoluminescence images of carbon antisite-vacancy pairs in 4H-SiC before and after inorganic passivation. a) Typical scanning confocal photoluminescence image for an unpassivated Si-face 4H-SiC substrate. b) Scanning confocal photoluminescence image for an Si-face 4H-SiC substrate with an AlN epilayer. c) Typical scanning confocal photoluminescence image for the unpassivated C face of a 4H-SiC substrate. d) Scanning confocal photoluminescence image for the C face of a 4H-SiC substrate passivated with an AlN epilayer. A significant increase in defect photoluminescence is observed after passivation. The inset shows a second order autocorrelation function ($g^2(\tau)$) measurement for a CAV center under an AlN passivation layer. The dip near a time delay of zero suggests the presence of single-photon emitters amidst a background from densely packed surrounding emitters. The $g^2(\tau)$ plot was normalized to the count level at a time delay value \approx 100 ns from the central dip. All images were collected with an excitation wavelength of 532 nm and a power of 3 mW. The color scale is the same for all panels.

count level from 0.08 ± 0.47 (N=51) to 0.90 ± 0.39 (N=50) after AlN passivation. Absolute count values also increase substantially following AlN passivation, particularly for 660 nm excitation (Figure S8, Supporting Information). The mean count level for CAVs increases from 24.6 ± 6.3 kcounts s⁻¹ to 78.5 ± 25.8 kcounts s⁻¹ for 532 nm excitation and from 8.8 ± 3.1 kcounts s⁻¹ to 29.2 ± 11.7 kcounts s⁻¹ for 660 nm excitation. The significantly lower count rate observed under 660 nm excitation as compared with 532 nm excitation is likely due to the fact that we use a 692 nm long pass filter to remove reflected laser light and this filter also removes a substantial portion of the PL signal (Figure S8, Supporting Information). All data were taken with a fixed incident laser power and do not distinguish between a change in ionization rate and a change in steady-state populations.

Photostability was further analyzed by quantifying the amount of time (out of the 60~s time interval of the measurement) each

emitter spends in an "off" state outside of a tolerance range based on photon shot noise. Statistically, approximately 99.7% of measured count values for each sampling interval should fall within the range $\lambda t \pm 3(\lambda t)^{1/2}$, where λ is the average count rate for the "on" state of each emitter and *t* is the sampling time, equal to 5 ms in our experiments (see the Supporting Information). The amount of time outside this range, defined as $\tau_{\rm off}$, provides a quantitative metric for count rate variability that originates from blinking/photobleaching and other intrinsic sources of instability. Analysis of the time traces collected under 532 nm excitation indicates rapid photobleaching (typically <1 s) for nearly all emitters, leading to a $\tau_{\rm off}$ value of 58.4 \pm 5.9 s (Figure S9, Supporting Information). Upon AlN passivation, substantial improvement in CAV photostability was observed under 532 nm excitation, as signified by the $\tau_{\rm off}$ value of 31.6 \pm 11.9 s. The analysis of the data under 660 nm excitation shows similar improvements, as illustrated by the change in $\tau_{\rm off}$ values from 55.5 \pm 8.0 s (for unpassivated C-face centers) to 13.5 \pm 11.2 s for AlN-passivated centers.

As discussed previously, upon AlN passivation, the PL from C-face centers increases, whereas the Si-face PL decreases markedly (Figure 2). This difference in behavior can be understood by considering the polar nature of AlN/4H-SiC heterojunctions. In a heterostructure grown parallel to the polar [0001] axis, a large mismatch in spontaneous polarization exists between the 4H-SiC substrate $(P_s = -2.16 \ \mu C \ cm^{-2})$ and the AlN epilayer $(P_s = -9.0 \ \mu C \ cm^{-2}).^{[24,25]}$ In addition, the misfit strain between the AlN epilayer and the substrate results in an additional piezoelectric polarization. Schematic illustrations of the structures and polarization components for both Si and C-face heterostructures

are shown in **Figure 4**a,b, respectively. In this situation,^[25] the interfacial sheet charge can be expressed as follows

$$\sigma = \left(P_{s}^{\text{SiC}} + P_{\text{piezo}}^{\text{SiC}}\right) - \left(P_{s}^{\text{AlN}} + P_{\text{piezo}}^{\text{AlN}}\right) \tag{1}$$

Here, the $P_{\rm s}$ and $P_{\rm piezo}$ terms represent the spontaneous and piezoelectric polarizations, respectively. The piezoelectric contribution from the relaxed SiC substrate is zero, and the piezoelectric contribution from the AlN epilayer, which we assume to be pseudomorphic, can be expressed as follows

$$P_{\text{piezo}}^{\text{AlN}} = 2d_{31}\varepsilon_1 \left(C_{11} + C_{12} - 2\frac{C_{13}^2}{C_{33}} \right)$$
 (2)

Here, the piezoelectric constant d_{31} for AlN is -2.65×10^{-12} C m⁻² Pa⁻¹, and the elastic constants for AlN are: $C_{11} = 410 \times 10^9$ Pa, $C_{12} = 140 \times 10^9$ Pa, $C_{13} = 100 \times 10^9$ Pa, and

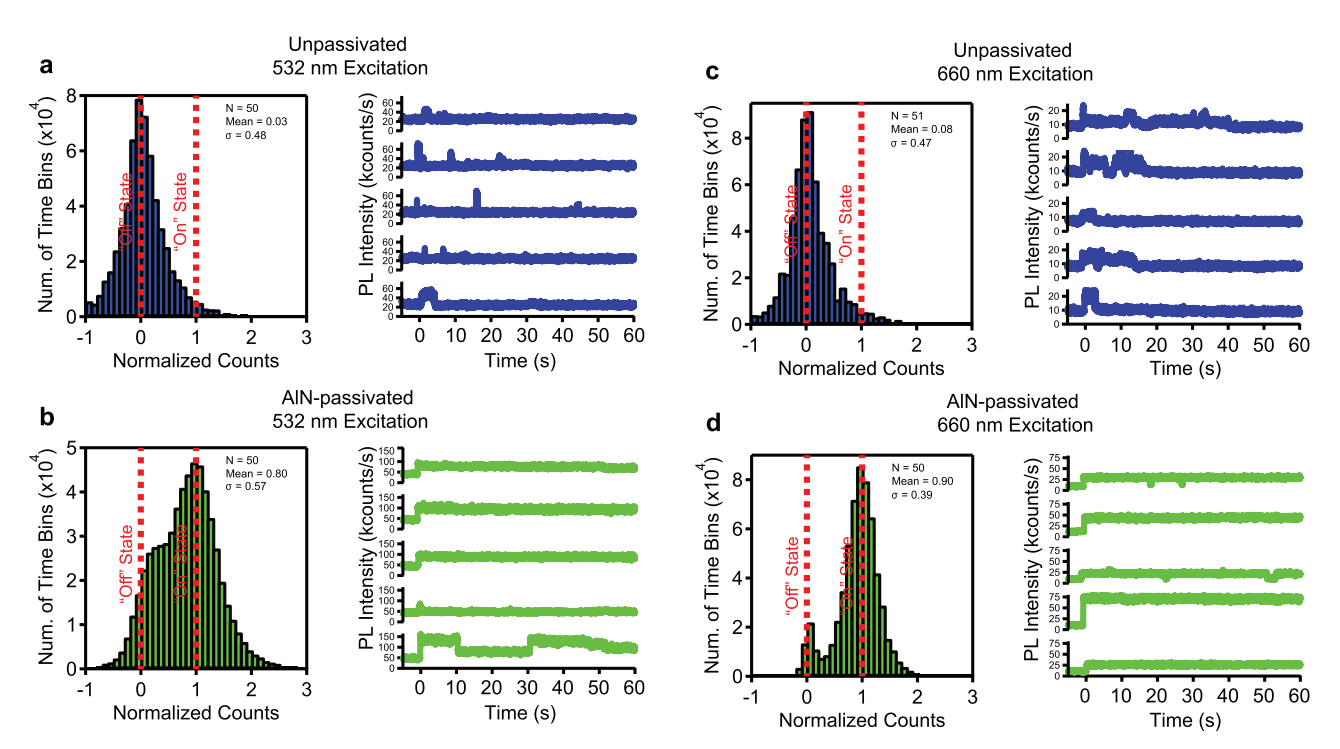


Figure 3. Composite normalized count histograms and sample time traces for CAV centers before and after AlN passivation. A value of zero corresponds to the background level, and a value of one corresponds to the "on" state count level. These levels are denoted with red lines for clarity. a) Composite normalized count histogram for all time traces collected for unpassivated C-face CAVs under 532 nm excitation (left) and corresponding representative time traces (right). b) Composite normalized count histogram for all time traces collected for AlN-passivated C-face CAVs under 532 nm excitation (left) and corresponding representative time traces (right). c) Composite normalized count histogram for all time traces collected for unpassivated C-face SiC under 660 nm excitation (left) and corresponding representative time traces (right). d) Composite normalized count histogram for all time traces collected for AlN-passivated C-face SiC under 660 nm excitation (left) and corresponding representative time traces (right). The large improvement in normalized count level, particularly under 660 nm excitation, reflects the large improvement in photostability after AlN passivation. The data in these histograms represent normalized count values obtained from time traces of $N \approx 50$ separate CAVs collected over 60 s with a binning time of 5 ms, and σ denotes the standard deviation of the normalized counts. All data were acquired with an excitation power of 3 mW. The time traces have been smoothed with a moving average for clarity. The jump in count rate near ≈ 0 s in all panels corresponds to the point at which the laser spot was placed on the defect center.

 $C_{33}=390\times 10^9~{\rm Pa.^{[25,26]}}$ The epitaxial strain ε_1 can be expressed as follows

$$\varepsilon_1 = \frac{a_{\text{SiC}} - a_{\text{AlN}}}{a_{\text{AN}}} \tag{3}$$

The lattice parameters for SiC and AlN are: $a_{SiC} = 3.073 \text{ Å}$; $a_{AlN} = 3.11$ Å. These calculations indicate that the epitaxial AlN layer should switch the sign of the sheet charge at the SiC surface, leading to a net negative sheet charge of $-3.7 \,\mu\text{C cm}^{-2}$ for the C face. Although the interfacial charge is likely reduced due to the presence of interfacial defects, an accumulation of holes is expected near the C face to compensate this sheet charge. The CAV center, which is responsible for visible light emission, is positively charged, [2,27] and thus the passivation-induced charge accumulation should lead to preferential stabilization of the emissive CAV centers on the C face after AlN passivation. This polarization-induced mechanism thus explains the increase in PL intensity of the C-face heterostructure upon AlN passivation in Figure 2. For the Si face, in contrast, an interfacial sheet charge of equal magnitude but opposite (positive) polarity is expected, leading to an accumulation of electrons near the interface. This charge accumulation can destabilize the positive charge state of CAVs, resulting in the observed suppression of PL for Si-face centers.

Through the patterning of the AlN epilayer, this polarization effect can be used to achieve spatial control of defect emission. As shown in Figure 4c,d, regions of a C-face SiC/AlN heterostructure in which the AlN passivation layer is removed via KOH etching exhibit greatly reduced PL intensity relative to the areas with an intact AlN epilayer. Control scans taken before and after KOH exposure (Figure S10, Supporting Information) indicate that this difference indeed stems from the epilayer removal and not from the KOH exposure. This polarization effect should provide a promising new route for stabilizing/destabilizing a defect-center charge state and thus for controlling the emission of color centers in SiC and other materials.

In addition to controlling the charge state of the defect center, AlN passivation also alters the photostability of a given charge state (Figure 3). This can be understood by examining the energy levels of the localized defect states with respect to the band edges of both the 4H-SiC host and the AlN epilayer. For the AlN/SiC system, previous calculations indicate that the excited state of CAV centers lies within 0.05 eV of the conduction band minimum, allowing for thermal excitation of

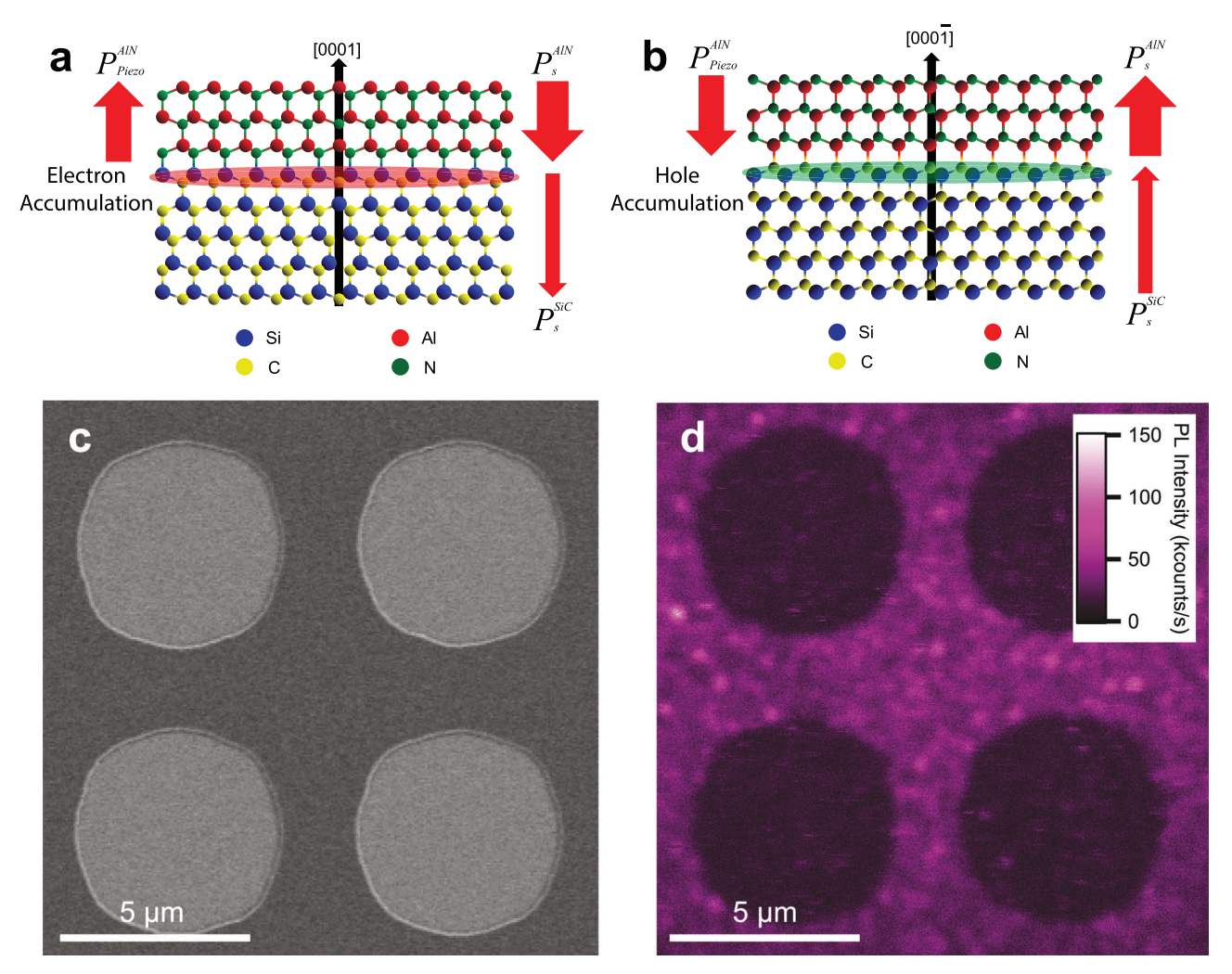


Figure 4. Spatially selective polarization-induced stabilization of the emissive positive charge state for CAVs in 4H-SiC. a) Schematic illustration of the structure of an Si-face heterostructure of AlN on 4H-SiC. The spontaneous polarization mismatch between 4H-SiC and AlN leads to an accumulation of electrons for an Si-face heterostructure. b) Schematic illustration of the structure of a C-face heterostructure of AlN on 4H-SiC. The spontaneous polarization mismatch in this case can be expected to lead to an accumulation of holes near the junction, leading to stabilization of the positive charge state of CAV centers. c) Scanning electron microscope image of an AlN epilayer on a C-face SiC substrate patterned by KOH etching. d) Scanning confocal photoluminescence image of the same patterned AlN-passivated C-face SiC substrate illustrated in panel (c). The PL intensity is greatly enhanced in regions with an intact AlN passivation layer (corresponding to the region outside the patterned circles).

electrons into the SiC conduction band.^[2] In addition, excitation at 532 nm can result in direct excitation of electrons from the CAV ground state into the conduction band.^[2] The migration of these photoexcited carriers to the surface and subsequent charge trapping is often considered a cause for pronounced photobleaching/blinking.^[12,28] The improvement in photostability observed after AlN passivation is consistent with a reduction in surface traps as compared to the unpassivated surfaces. This is analogous to the protection of emissive states in core—shell quantum dots.^[16] The enhanced photostability of the CAV centers under 660 nm laser excitation can be attributed to the reduced photoionization of CAVs.^[2]

As core–shell passivation schemes have resulted in dramatic improvements in the luminescence properties of quantum dots, inorganic passivation schemes may yield similar improvements

in the optical properties of solid-state defect centers. Further improvements may be achieved through growth of higher quality films by techniques such as MBE.^[19] Inorganic passivation schemes may also be extended to other types of single photon-emitting defect systems in other materials, including infrared-emitting defects observed in 4H and 6H-SiC^[4–6] and color centers in diamond.^[1] Cubic boron nitride, which has a small lattice mismatch with diamond (3.62 Å for boron nitride vs. 3.57 Å for diamond), has particular promise for epitaxial passivation of diamond defect centers.^[29] The present results demonstrate the promise of epitaxial inorganic passivation schemes for defect-based quantum emitters and pave the way to bright, environmentally robust single-photon emitters with superior photostability and permanent, spatially selective charge state control.

www.advancedsciencenews.com



www.advmat.de

Experimental Section

Sample Preparation: High-purity semi-insulating 4H-SiC wafers were purchased from Cree Inc. Wafers with a chemical-mechanical polish on either the Si or C face (part numbers W4TRE0R-0200 and W4TRE0R-0600, respectively) were used for analysis of the Si and C faces. The as-received wafers were irradiated at an energy of 2 MeV and a dose of 10¹² cm⁻² by Neo Beam Ltd. at Kent State University. The irradiated wafers were diced, and the chips were ultrasonically cleaned in acetone and 2-propanol, cleaned with 2:1 piranha (H₂SO₄:H₂O₂) for 10 min, and etched with concentrated HF for 2 min. The samples were then etched in an STS ICP reactive ion etcher using a mixture of CF₄ (30 sccm) and O_2 (15 sccm) at a chamber pressure of 15 mtorr, an RF power of 900 W, and a platen power of 50 W for 10 min to remove polishing damage. The samples were then cleaned using the same procedure with acetone, 2-propanol, piranha, and HF and annealed under constant Ar flow for 20 h at 800 °C in a quartz tube furnace. The samples were then cleaned with piranha (10 min) and etched with HF (2 min) to remove any contaminants and surface oxide created during the anneal.

Epilayer Growth: Films of AIN were grown using RF sputtering of an AIN target (AJA International) with an AJA International Orion 3 sputtering system. Films were grown for 5 min at a power of 150 W, a pressure of 4 mtorr, and a temperature of 500 °C. Gas flow rates for the process were 19/1 sccm of Ar/N₂, and a base pressure less than 5×10^{-7} torr was attained before the deposition. The SiC substrates were cleaned with concentrated HF (2 min) prior to the deposition to remove any native oxide.

Film Characterization: FTIR reflectance measurements on AIN films were acquired at an angle of 45° using a Perkin Elmer Spectrum One spectrometer equipped with a Pike Technologies VeeMax II variable angle reflectance unit. Samples for transmission electron microscopy (TEM) were prepared using a Zeiss NVision 40 focused ion beam system (FIB) equipped with an Omniprobe mechanical probe. Samples were coated with a protective layer consisting of $\approx\!50$ nm of Ti and $\approx\!1$ μm of Ag or Au using DC sputtering, milled using the FIB, and lifted out with an Omniprobe tip. Samples were attached to Omniprobe TEM grids, thinned, and polished using the FIB beam. AIN films were imaged using a JEOL 2010-F TEM operated at 200 kV and equipped with a field emission gun and an AMT charge-coupled device.

Scanning Confocal PL Measurements: PL measurements were taken using a home-built scanning confocal microscope under both 532 and 660 nm laser excitation in a 3 mW diffraction-limited spot using an air objective (150 \times and NA = 0.9). For analysis of CAV centers and $g^2(\tau)$ measurements, the PL signal was filtered through a 532 nm notch filter, 594 nm dichroic mirror, and 600 nm long pass filter, then collected via single-mode optical fibers and detected using Perkin Elmer SPCM-AQR-14-FC single photon-counting avalanche photodiodes. Measurements of CAV centers with 660 nm excitation were completed using a 660 nm diode laser and PL was collected through a 677 nm dichroic mirror and a 692 nm long pass filter. Spectra were collected using a 300 lines mm $^{-1}$ grating and a Princeton Instruments PIXIS charge-coupled device.

AIN Patterning: After deposition of an AIN film, an $\mathrm{Si_3N_4}$ mask was deposited using an STS PECVD system. The mask was written into PMMA using conventional electron beam lithography, and the pattern was transferred to the $\mathrm{Si_3N_4}$ using HF. Subsequent etching of the AIN layer was achieved by immersion in a 70% KOH solution for 10 min followed by a 5 min HF etch to remove the $\mathrm{Si_3N_4}$ mask layer.

Supporting Information

Supporting Information is available from the Wiley Online Library or from the author.

Acknowledgements

The authors gratefully acknowledge Edwin Macomber, Nicholas Antoniou, and Adam Graham for technical assistance, and Evelyn Hu and

Adam Gali for helpful discussions. Funding for this work was provided by the ONR Vannevar Bush Fellowship (N00014-16-1-2825), ARL CDQI (W911NF1520067), and DARPA SPARQC (W31P4Q-12-1-0017). This work was performed in part at the Center for Nanoscale Systems (CNS), a member of the National Nanotechnology Infrastructure Network (NNIN).

Conflict of Interest

The authors declare no conflict of interest.

Keywords

color centers, epitaxial films, photoluminescence, quantum emitters, silicon carbide

Received: August 10, 2017 Revised: October 6, 2017 Published online: December 5, 2017

- [1] F. Jelezko, J. Wrachtrup, Phys. Status Solidi A 2006, 203, 3207.
- [2] S. Castelletto, B. C. Johnson, V. Ivády, N. Stavrias, T. Umeda, A. Gali, T. Ohshima, *Nat. Mater.* 2014, 13, 151.
- [3] G. Balasubramanian, P. Neumann, D. Twitchen, M. Markham, R. Kolesov, N. Mizuochi, J. Isoya, J. Achard, J. Beck, J. Tissler, V. Jacques, P. R. Hemmer, F. Jelezko, J. Wrachtrup, *Nat. Mater.* 2009, 8, 383.
- [4] W. F. Koehl, B. B. Buckley, F. J. Heremans, G. Calusine, D. D. Awschalom, *Nature* 2011, 479, 84.
- [5] M. Widmann, S. Y. Lee, T. Rendler, N. T. Son, H. Fedder, S. Paik, L. P. Yang, N. Zhao, S. Yang, I. Booker, A. Denisenko, M. Jamali, S. A. Momenzadeh, I. Gerhardt, T. Ohshima, A. Gali, E. Janzen, J. Wrachtrup, *Nat. Mater.* 2015, 14, 164.
- [6] D. J. Christle, A. L. Falk, P. Andrich, P. V. Klimov, J. U. Hassan, N. T. Son, E. Janzen, T. Ohshima, D. D. Awschalom, *Nat. Mater.* 2015, 14, 160.
- [7] M. V. Gurudev Dutt, L. Childress, L. Jiang, E. Togan, J. Maze, F. Jelezko, A. S. Zibrov, P. R. Hemmer, M. D. Lukin, *Science* 2007, 316, 1312.
- [8] E. Togan, Y. Chu, A. S. Trifonov, L. Jiang, J. Maze, L. Childress, M. V. Dutt, A. S. Sorensen, P. R. Hemmer, A. S. Zibrov, M. D. Lukin, *Nature* 2010, 466, 730.
- [9] J. R. Weber, W. F. Koehl, J. B. Varley, A. Janotti, B. B. Buckley, C. G. Van de Walle, D. D. Awschalom, *Proc. Natl. Acad. Sci. USA* 2010, 107, 8513.
- [10] Y. R. Chang, H. Y. Lee, K. Chen, C. C. Chang, D. S. Tsai, C. C. Fu, T. S. Lim, Y. K. Tzeng, C. Y. Fang, C. C. Han, H. C. Chang, W. Fann, Nat. Nanotechnol. 2008, 3, 284.
- [11] G. Kucsko, P. C. Maurer, N. Y. Yao, M. Kubo, H. J. Noh, P. K. Lo, H. Park, M. D. Lukin, *Nature* 2013, 500, 54.
- [12] M. Kaviani, P. Deak, B. Aradi, T. Frauenheim, J. P. Chou, A. Gali, Nano Lett. 2014, 14, 4772.
- [13] M. V. Hauf, B. Grotz, B. Naydenov, M. Dankerl, S. Pezzagna, J. Meijer, F. Jelezko, J. Wrachtrup, M. Stutzmann, F. Reinhard, J. A. Garrido, *Phys. Rev. B* 2011, 83, 081304(R).
- [14] L. M. Struck, M. P. D'Evelyn, J. Vac. Sci. Technol., A 1993, 11, 1992.
- [15] R. E. Thomas, R. A. Rudder, R. J. Markunas, J. Vac. Sci. Technol., A 1992, 10, 2451.
- [16] X. Peng, M. C. Schlamp, A. V. Kadavanich, A. P. Alivisatos, J. Am. Chem. Soc. 1997, 119, 7019.



www.advancedsciencenews.com



www.advmat.de

- [17] T. Umeda, N. T. Son, J. Isoya, E. Janzén, T. Ohshima, N. Morishita, H. Itoh, A. Gali, M. Bockstedte, Phys. Rev. Lett. 2006, 96, 145501.
- [18] J. Choi, R. Puthenkovilakam, J. P. Chang, Appl. Phys. Lett. 2005, 86, 192101.
- [19] N. Onojima, J. Suda, H. Matsunami, Jpn. J. Appl. Phys. 2003, 42, 445
- [20] M. Kim, J. Ohta, A. Kobayashi, H. Fujioka, M. Oshima, Appl. Phys. Lett. 2007, 91, 151903.
- [21] C. Xiong, W. H. Pernice, H. X. Tang, Nano Lett. 2012, 12, 3562.
- [22] M. Bickermann, B. M. Epelbaum, P. Heimann, Z. G. Herro, A. Winnacker, Appl. Phys. Lett. 2005, 86, 131904.
- [23] R. A. Youngman, J. H. Harris, J. Am. Ceram. Soc. 1990, 73, 3238.

- [24] V. M. Polyakov, F. Schwierz, J. Appl. Phys. 2005, 98, 023709.
- [25] O. Ambacher, V. Cimalla, Polarization Effects in Semiconductors: From Ab Initio Theory to Device Applications, Springer, New York, USA 2008.
- [26] L. E. McNeil, M. Grimsditch, R. H. French, J. Am. Ceram. Soc. 1993, 76, 1132.
- [27] T. Umeda, J. Ishoya, T. Ohshima, N. Morishita, H. Itoh, A. Gali, Phys. Rev. B 2007, 75, 245202.
- [28] C. Bradac, T. Gaebel, N. Naidoo, M. J. Sellars, J. Twamley, L. J. Brown, A. S. Barnard, T. Plakhotnik, A. V. Zvyagin, J. R. Rabeau, Nat. Nanotechnol. 2010, 5, 345.
- [29] W. J. Zhang, X. M. Meng, C. Y. Chan, K. M. Chan, Y. Wu, I. Bello, S. T. Lee, J. Phys. Chem. B 2005, 109, 16005.